

# Nested mesoscale to large-eddy simulations for wind energy applications

Nikola Marjanovic <sup>a</sup>, Fotini Katopodes Chow <sup>b</sup>, Julie K. Lundquist <sup>c</sup>

<sup>a</sup>*University of California, Berkeley, Berkeley, California, USA, nikola\_marjanovic@berkeley.edu*

<sup>b</sup>*University of California, Berkeley, Berkeley, California, USA, tinakc@berkeley.edu*

<sup>c</sup>*University of Colorado at Boulder, Boulder, Colorado, USA, Julie.Lundquist@colorado.edu*

**ABSTRACT:** Wind turbine micrositing, operational wind power forecasting, and turbine design require high-resolution simulations of atmospheric flow over complex terrain. We are developing large-eddy simulations (LES) for wind energy applications using the Weather Research and Forecasting (WRF) model. Grid nesting is used to refine the grid from mesoscale to finer scales which can adequately resolve terrain and turbulence in the atmospheric boundary layer. In this study, we examine the performance of the grid nesting configuration, horizontal and vertical resolution, and turbulence closures for simulations of wind ramping events at a West Coast North America wind farm. The ultimate goal of this work is to accurately simulate the physical processes important to a wind farm such as ramping and high shear events.

## 1 INTRODUCTION

The current difficulty with wind power forecasting is the inability to accurately predict the occurrence and intensity of atmospheric conditions at the heights spanned by industrial-scale turbines (40-160m). With better simulation of the relevant physics, operational practices such as integration of large fractions of wind power into power grids, scheduling maintenance on wind energy facilities, and defining design criteria for next-generation turbines and siting will be made possible. High-resolution simulations of the atmospheric boundary layer have become more practical with increases in available computational power. For accurate simulations, however, the model operator is required to make choices regarding model grid spacing, turbulence parameterization, land surface representations and the configuration of initial and lateral boundary conditions. The “proper” choice of these parameters is highly dependent on the situation under consideration.

This paper investigates the steps necessary to achieve accurate simulations of the wind fields and “ramping” events at a wind farm near the western coast of the United States. “Ramping” refers to a rapid increase in wind speed over a short period of time and is of great interest to wind farm operators for predicting power output as well as preventing turbine fatigue. The exact definition of a ramping event varies in practice; examples include a 20% capacity change in production over a thirty-minute period (Freedman et al. 2008), or a pre-specified change in the magnitude of system-wide production. Ramping events specifically driven by meteorology may be able to be captured by a good meso-scale meteorological model.

The predictability of ramping events depends largely on the atmospheric conditions causing the event. Meteorologically-driven ramping events may be due to atmospheric motions at several scales. For example, thermally-driven winds such as sea breezes, mountain-valley circulations, or low-level jets occur at local scales, whereas the passage of a cold front is a synoptically driven phenomenon. In all cases, associated wind transitions simply appear as large ramps in the wind speed time series to wind farm systems operators, though the cause for the wind changes can be quite different. Larger, synoptically driven features have longer time scales and are more straight-

forward to forecast than local-scale phenomena, which usually require fine scale information about land-surface conditions and turbulent mixing in the atmosphere.

The wind farm which is the focus of this study covers an area of about 10 km by 10 km with a fairly flat topography that includes a few hills with elevation changes less than 150 m. Observation data is available from a sodar, two meteorological towers and cup anemometers on the turbine nacelles that can be used for comparison to numerical simulations. We use the Weather Research and Forecasting (WRF) model as our simulation tool (Skamarock and JB Klemp 2008). It is intended mainly for mesoscale atmospheric simulations and includes large-eddy simulation (LES) capabilities. WRF has a fully compressible, Eulerian and nonhydrostatic equation set. This work focuses on the numerical aspects of the simulation needed to accurately represent the flow over the wind farm.

Here we examine one ramping event to develop preliminary insight into the ability of WRF to capture shifts in wind speed that are important to wind farm operators. This particular ramping event falls in the category of synoptically-driven transitions and hence should be the easiest to predict if the large-scale meteorological forcing is correct. Many studies over complex terrain point to increasing grid resolution as a means to achieving better agreement of simulations with observations (see e.g. (Gronas & Sandvik 1999; Grell et al. 2000). Errors in wind speed and direction can also be due to errors in the representation of turbulent motions, as well as to subgrid features in the topography and land use, as seen in the simulations of (Hanna and Yang 2001). The effects of horizontal and vertical grid resolution, one-way vs. two-way nesting, domain size, and turbulence closure models are examined here. Preliminary results are presented below, along with discussion of the numerical setup and grid nesting approaches.

## 2 NUMERICAL SIMULATION SETUP

### 2.1 *Grid nesting and topography*

Four two-way nested grids were used to simulate flow conditions for the wind farm at horizontal resolutions of 8.1 km, 2.7 km, 900 m, and 300 m. The main features of the topography are visible on the 900 m grid, but its fine structure becomes much better resolved at 300 m resolution. Topography for the 8.1 km and 2.7 km grids was obtained using the USGS 30 arc second topography datasets. For the 900 m through 300 m grid resolution simulations, the topography was extracted from a 10 m resolution dataset available for California from USGS. The terrain is smoothed near the boundary for each nested subdomain to match the elevations from the surrounding coarser grids. WRF uses a terrain-following, hydrostatic-pressure vertical coordinate system with the top of the model being a constant pressure surface. The vertical grid spacing is normally assigned by default, or can be user specified to decrease spacing near the bottom of the model and increase it near the top. The minimum vertical grid spacing ( $\Delta z_{\min}$ ) at the surface, as well as the average spacing ( $\Delta z_{\text{avg}}$ ), are listed in Table 1 for our grid configurations. The domain height ( $\sim 13$  km) is near the tropopause in all cases. The horizontal spacing ( $\Delta h$ ) is uniform in both directions. Because of WRF's stability conditions, increases in spatial resolution require similar increases in model timestep, as seen in Table 1.

Table 1. Simulation parameters for each grid level

$(n_x, n_y, n_z)$	$\Delta h$ (m)	$\Delta z_{\min}, \Delta z_{\text{avg}}$ (m)	$\Delta t$ (s)
(96,96,49)	8100	35, 246	30
(96,96,49)	2700	35, 246	10
(96,96,49)	900	35, 246	3.33
(96,96,49)	300	35, 246	1.11

## 2.2 Initialization and lateral boundary conditions

Initial and boundary conditions are obtained from the National Center for Atmospheric Research's (NCAR) North American Regional Reanalysis (NARR) data. NARR is resolved at 32 km horizontally at 29 vertical levels (1000-100hPa; excluding surface) to force the WRF simulations at the coarsest grid. Lateral boundary condition forcing was applied at three-hour intervals and linearly interpolated in between. Relaxation towards the lateral boundary values was applied around the edge of the domain. Simulations were performed for 48 hours beginning 20 hours before the ramping event; output was stored at five-minute intervals and used to generate initial and boundary conditions files during the simulation for the nested grids.

## 2.3 Surface characteristics

WRF uses 33 land use categories (including water and ice) from USGS. WRF incorporates land use data from USGS 30 second global data for 2.7 km and coarser grids. The high resolution grids (900 m and finer) use National Land Cover Database (NLCD) data at 30 m resolution. This dataset includes 19 land use categories, which have been mapped to the USGS categories used by WRF. The Noah Land Surface Model is used with initial soil temperature and moisture in four layers provided from NARR. At fine resolutions it may be necessary to use finer-scale soil initialization fields; this will be investigated in future work to consider land-atmosphere coupling effects on the boundary layer (Woodward et al. 2009; Williams et al. 2009).

## 2.4 Turbulence and computational mixing

The standard Mellor-Yamada-Janjic scheme (appropriate for Reynolds-Averaged Navier-Stokes simulations) is used for the base case. Mellor-Yamada-Janjic (MYJ) is a one-dimensional prognostic turbulent kinetic energy scheme with local vertical mixing. The TKE closure of order 1.5 is used for the large-eddy-simulations performed. The TKE-1.5 model is useful in an LES context as long as the chosen length scale is proportional to the filter width, as it is in WRF. This closure is particularly useful for LES when a large fraction of the velocity scales are contained in the subfilter scales as with coarse resolution grids. Other LES closures will be used for comparison in the future, including the Dynamic-Wong-Lilly (DWL) model and Dynamic Reconstruction Models (DRM) (Chow et al. 2005), which have been implemented into WRF (Mirocha et al. 2007).

## 3 COMPARISON WITH OBSERVATION DATA

Results comparing simulations with observation data for the ramping event are given in this section. The event is caused by a frontal passage just after significant precipitation and appears about 10 hours into the day at which point wind speed magnitude more than doubles. The naming convention for runs is “(finest horizontal resolution)\_(number of points in vertical)” (see Table 2). All results are from two-way nesting and the Mellor-Yamada-Janjic turbulence model unless otherwise noted.

Table 2. Simulation configurations

Run name	Configuration
300m_49	reference simulation set, 4 two-way nested grids
300m_70	4 two-way nested grids with 70 vertical levels
300m_40	4 two-way nested grids with 40 vertical levels (chosen by WRF)

300m_49_1way	4 one-way nested grids
900m_49_1way	3 one-way nested grids
2700m_49_1way	2 one-way nested grids
8100m_49_1way	single grid
300m_49_TKE1.5	4 one-way nested grids, with TKE1.5 closure on 2 finest grids

### 3.1 Effects of horizontal resolution

The effect of horizontal resolution was investigated to determine if it is significant in simulating this particular synoptically-induced ramping event. We compare output from the same one-way nested runs to evaluate the impact of grid resolution. SODAR observations of the evolution of wind speed and wind direction 80 m above the surface during the ramping event are presented in Figure 1. The observations are compared to the one-way nested run resolutions: 300m\_49\_1way (4 grid nests), 900m\_49\_1way (3 grid nests), 2700m\_49\_1way (2 grid nests), and 8100m\_49\_1way (1 grid). Regardless of resolution, the simulation shows an increase in wind speed associated with this ramp that is more gradual than was observed by the SODAR.

Figure 2 shows vertical profiles of the ramping event. In general, the simulations better capture the wind speed after ramping rather than before it, and wind direction is better predicted after the ramping. SODAR data are available at 10 m intervals from 20 – 200 m above ground level, however at elevations above 100m there is usually little data available.

To further quantify the comparison, Table 3 shows the root-mean-square errors (RMSE) and mean absolute errors (MAE) between the SODAR data and the simulations over 0-200 m above the ground, averaged over 24 hours. They are defined as:

$$MAE = \frac{1}{M} \sum_{j=1}^M \frac{1}{N} \sum_{i=1}^N |A_{i,j} - B_{i,j}| \quad (1)$$

$$RMSE = \sqrt{\frac{1}{M} \sum_{j=1}^M \frac{1}{N} \sum_{i=1}^N (A_{i,j} - B_{i,j})^2} \quad (2)$$

where M = number of time steps; N = number of vertical grid points; A = observation; and B = simulation data.

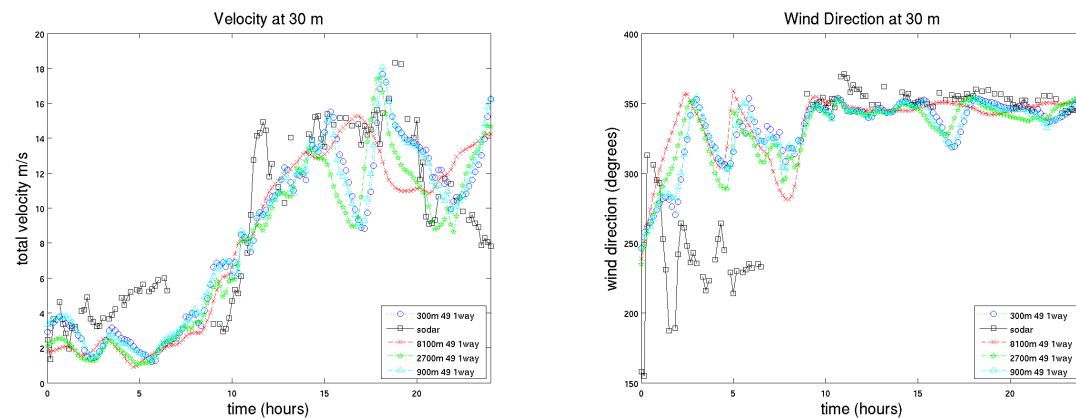


Figure 1: Total wind speed and wind direction time series during ramping event (24 hour period) for different horizontal resolutions (grid nesting levels).

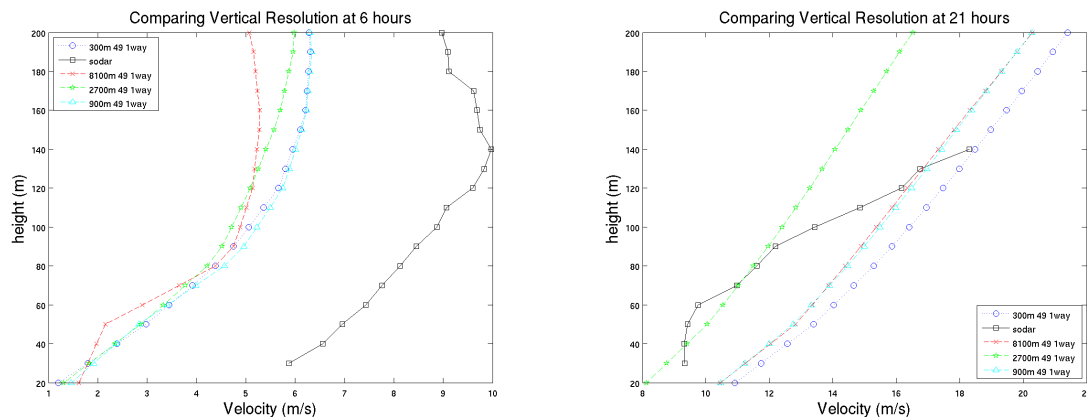


Figure 2: Total wind speed vertical profiles before (left) and after (right) the ramping event for different horizontal resolutions (grid nesting levels).

Table 3. RMSE and MAE for wind speed and direction for different horizontal resolutions (grid nesting levels).

Grid	U (m/s)		$\phi$ ( $^{\circ}$ )	
	RMSE	MAE	RMSE	MAE
300m_49	3.50	2.70	69.90	50.08
900m_49	3.58	2.74	70.33	50.59
2700m_49	3.27	2.52	69.63	50.41
8100m_49	3.09	2.43	73.16	51.55

The difference between the errors for the various grid resolutions is not very significant, as seen in the error metrics listed in Table 3. The results are slightly skewed towards the coarser resolution because of the coarser grid giving results closer to the observations after the ramping event, which occurs over a longer portion of the averaging period. While all of the runs capture the increase in wind speed during the ramping event itself, none of the simulations capture the shift in wind direction. Under these particular conditions where the ramping is synoptically forced, relatively coarse horizontal resolution (8.1 km) appears to be adequate in capturing the shift in wind speed at the wind turbine hub heights (~80-100 m). We caution that this conclusion is probably not applicable to other ramping events due to different meteorological processes.

### 3.2 Effects of vertical resolution

Vertical spacing may have a significant effect on the accuracy of wind speed and direction predictions when wind shear is strong, e.g. in the case of nocturnal low level jets which can also be responsible for ramping events (see e.g. Storm et al. 2009). The vertical grids tested here using 4 two-way nesting levels were generated as follows: 300m\_49 uses a *tanh* function to stretch the vertical grid spacing so that there is smaller spacing closer to the ground; 300m\_70 uses specified grid levels that provide spacing of about 10 m in the lowest 200 m of the atmosphere and then stretched; 300m\_40 was created by specifying 40 levels in WRF and using the default spacing (the minimum spacing was 60 m and average spacing was 309 m). Figure 3 shows the evolution of the wind speed and Table 4 shows the RMSE and MAE between simulations and observations along with the average vertical spacing in the range of the observation data (20-200m). The grids all give similar results for this ramping event. The 300m\_70 results, however, show a small improvement in capturing the rate of wind speed increase at the ramping event.

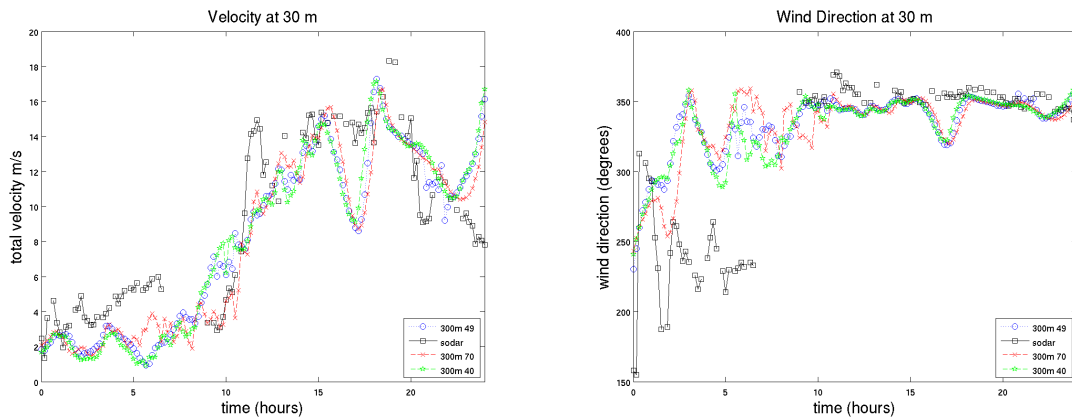


Figure 3. Total wind speed and wind direction time series during ramping event (24 hour period) for different vertical resolutions.

Table 4. RMSE and MAE for wind speed and direction for different vertical resolutions.

Grid	$\Delta z$ (m)	$U$ (m/s)		$\phi$ ( $^{\circ}$ )	
		RMSE	MAE	RMSE	MAE
300m_49	37.45	3.59	2.79	71.09	51.46
300m_70	9.87	3.10	2.41	68.38	48.78
300m_40	71.50	3.83	3.07	72.81	53.00

### 3.3 Difference between 1-way and 2-way nesting

With two-way nesting, the finer grid feeds back information to the coarser parent domain, thus updating the coarser grid with higher resolution fields and theoretically leading to a more accurate simulation. In one-way nesting, the finer domains do not influence the parent domains at all. Two-way nesting is thought to be important when fine-scale features that are resolvable on the finer domain affect meteorological conditions on a larger scale. Under strong synoptic-scale forcing, it is likely that one-way nesting will be adequate for feeding information from the larger scales to the finer grids. This hypothesis is confirmed for this ramping event in Figure 4, which shows the time series of wind speed and direction for our 2-way nested base case, 300m\_49, and the 1-way nested 300m\_49\_1way, each with the same four nesting levels. Table 5 shows the RMSE and MAE between simulations and observations. There is no significant difference between 1-way nesting and 2-way nesting in WRF's simulations compared to the observations.

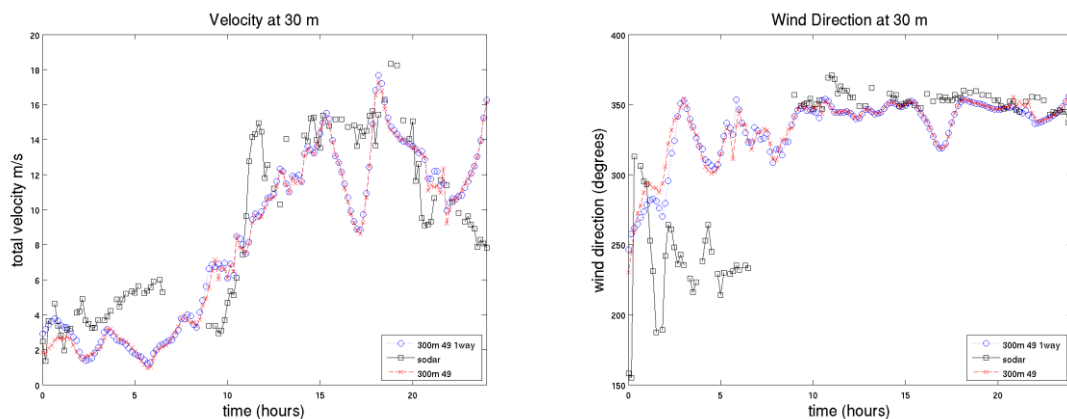


Figure 4. Total wind speed and wind direction time series during ramping event (24 hour period).

Table 5. Root-mean-square errors (rmse) and mean absolute errors (mae) for wind speed and direction per grid res.

Grid	U (m/s)		$\phi$ ( $^{\circ}$ )	
	RMSE	MAE	RMSE	MAE
300m_49	3.59	2.79	71.09	51.46
300m_49_1way	3.50	2.70	69.90	50.08

### 3.4 Comparing RANS to LES closures

At horizontal resolutions finer than 1 km, it may be beneficial to transition to a large-eddy simulation closure within a nested simulation framework. WRF’s standard LES closure is the TKE 1.5 scheme. We performed simulations using the TKE 1.5 turbulence model for the two finest domain levels and compared to the Mellor-Yamada-Janjic model. Both runs are 1-way nested because simulations with TKE 1.5 are unstable for 2-way nesting in this case (Moeng et al. 2007). Figure 5 and Table 6 both show that simulations using TKE1.5 significantly over predict wind speeds after the ramping event. Table 6 shows the RMSE and MAE values are much greater as a consequence. These results require further investigation to determine the cause of the velocity over-prediction.

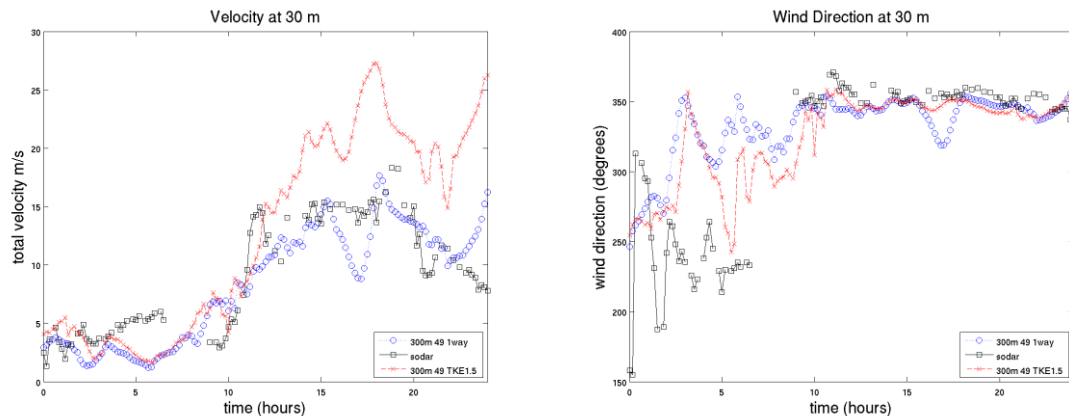


Figure 5. Total wind speed and wind direction time series during ramping event (24 hour period).

Table 6. Root-mean-square errors (rmse) and mean absolute errors (mae) for wind speed and direction per grid res.

Grid	U (m/s)		$\phi$ ( $^{\circ}$ )	
	Rmse	Mae	Rmse	Mae
300m_49_TKE1.5	6.43	4.37	70.45	49.54
300m_49_1way	3.50	2.70	69.90	50.08

## 4 CONCLUSIONS

This paper presents preliminary simulation results using WRF to capture a synoptically-driven ramping event at a wind farm on the west coast of the United States. The wind ramping was well represented with all grid resolutions and grid nesting configurations tested. Simulations of another ramping case (not shown) also indicated similar agreement of the model with observations regardless of the choice of grid resolution. These results seem counter-intuitive based on general recommendations to use higher resolution, but under certain synoptic conditions, the external forcing may be so strong during ramping that higher resolution offers no benefits. This is unlikely to be true under other meteorological conditions. It also remains unclear what turbulence clo-

sure approach (RANS vs. LES) is most appropriate at fine horizontal resolutions (Wyngaard 2004). Future work will investigate ramping events induced by other meteorological phenomena to determine when higher resolution and different turbulence models may be necessary.

## 5 ACKNOWLEDGEMENTS

The authors express great appreciation to Iberdrola Renewables, Inc., for the collection and provision of the observational data, and in particular Dr. Justin Sharp, Dr. Mike Zulauf, and Dr. Jerry Crescenti. This work was funded through Lawrence Livermore National Laboratory by the Department of Energy's Wind and Hydropower Technologies Program Office under the Renewable Systems Interconnect Support program managed by Mr. Stan Calvert. LLNL is operated by Lawrence Livermore National Security, LLC, for the DOE, National Nuclear Security Administration under Contract DE-AC52-07NA27344.

## 6 REFERENCES

- Chow, F. K., R. L. Street, M. Xue, and J. H. Ferziger. 2005. Explicit filtering and reconstruction turbulence modeling for large-eddy simulation of neutral boundary layer flow. *Journal of the Atmospheric Sciences* 62, no. 7: 2058-2077.
- Freedman, J., Markus, M., and Penc, R. 2008. Analysis of West Texas wind plant ramp-up and ramp-down events. AWSTruewind report.
- Grell, G. A., S. Emeis, W. R. Stockwell, T. Schoenemeyer, R. Forkel, J. Michalakes, R. Knoche, and W. Seidl. 2000. Application of a multiscale, coupled MM5/chemistry model to the complex terrain of the VOTALP valley campaign. *Atmos. Environ.* 34, no. 9: 1435 – 1453.
- Gronas, S., and A. D Sandvik. 1999. Numerical simulations of local winds over steep orography in the storm over north Norway on October 12, 1996. *J. Geophys. Res.* 104, no. D8: 9107-20.
- Hanna, S. R., and R. X. Yang. 2001. Evaluations of mesoscale models' simulations of near-surface winds, temperature gradients, and mixing depths. *J. Appl. Meteor.* 40, no. 6: 1095 – 104.
- Mirocha, J. D., F. K Chow, J. K. Lundquist, and K. A. Lundquist. 2007. Improved subfilter turbulence modeling for large eddy simulation using WRF. In *7th Symposium on the Urban Environment, American Meteorological Society*, Paper 13.1, 4 pages.
- Moeng, CH, J Dudhia, J Klemp, and P Sullivan. 2007. Examining two-way grid nesting for large eddy simulation of the PBL using the WRF model. *MONTHLY WEATHER REVIEW* 135, no. 6 (June): 2295-2311. doi:10.1175/MWR3406.1.
- Skamarock, WC, and JB Klemp. 2008. A time-split nonhydrostatic atmospheric model for weather research and forecasting applications. *JOURNAL OF COMPUTATIONAL PHYSICS* 227, no. 7 (March 20): 3465-3485. doi:10.1016/j.jcp.2007.01.037.
- Storm, B, J Dudhia, S Basu, A Swift, and I Giammanco. 2009. Evaluation of the Weather Research and Forecasting Model on Forecasting Low-level Jets: Implications for Wind Energy. *WIND ENERGY* 12, no. 1 (January): 81-90. doi:10.1002/we.288.
- Williams, J. L., Maxwell, R. M., Lundquist, J. K., and Wharton, S. 2009. On the use of a coupled variably-saturated groundwater flow - land surface model to initialize a fully coupled subsurface - land surface - atmospheric model for wind energy forecasting. *Eos Trans. AGU Fall Meeting Supplement* 90 (52): Abstract A31F-0183.
- Woodward, C. S., Maxwell, R. M., Lundquist, J. K., Mirocha, J., Smith, S., and Tompson, A. F. 2009. Wind Energy Resource Assessment Using Coupled Groundwater-Land-Surface Atmospheric Models. *Eos Trans. AGU Fall Meeting Supplement* 90 (52): Abstract A31F-0189.
- Wyngaard, J. C. 2004. Toward numerical modeling in the "Terra Incognita". *JAS* 61: 1816-1826.